

Lattice QCD study of generalized gluelumps

Kristen Marsh and Randy Lewis

*Department of Physics and Astronomy,
York University, Toronto, Ontario, M3J 1P3, Canada*

Proposals for physics beyond the standard model often include new colored particles at or beyond the scale of electroweak symmetry breaking. Any new particle with a sufficient lifetime will bind with standard model gluons and quarks to form a spectrum of new hadrons. Here we focus on colored particles in the octet, decuplet, 27-plet, 28-plet and 35-plet representations of $SU(3)$ color because these can form hadrons without valence quarks. In every case, lattice creation operators are constructed for all angular momentum, parity and charge conjugation quantum numbers. Computations with fully dynamical lattice QCD configurations produce numerical results for mass splittings within this new hadron spectrum. A previous quenched lattice study explored the octet case for certain quantum number choices, and our findings provide a reassessment of those early results.

I. INTRODUCTION

Quantum chromodynamics (QCD) describes the interactions between colored particles such as the color-triplet quarks and color-octet gluons of the standard model, but additional colored particles are present in many extensions of the standard model. Supersymmetry requires gluinos and squarks. String theory provides a broader range of possibilities. New strong dynamics would generate a spectrum of new composite particles (recall the technihadrons of classic technicolor), and if the new elementary particles (akin to techniquarks) carry QCD color, then the new composite particles occur as octets, decuplets, and other multiplets of QCD color. Studies of new colored particles in the context of the Large Hadron Collider therefore go far beyond triplets and octets [1–7], continuing several decades of interest in the range of color representations that might be realized beyond the standard model [8–25].

Lattice QCD is routinely used to obtain quantitative results from the $SU(3)$ gauge theory of gluons and quarks. The inclusion of additional particles in an octet [26–32], sextet [26, 33–40], or symmetric [41, 42] representation has also been investigated, in some cases applied to a new strong interaction rather than to QCD itself. Of more direct relevance to our work is a lattice study by Michael and coworkers [43–46], culminating in Ref. [46] where QCD is coupled to a new heavy color-octet particle representing the gluino of supersymmetry. Given that the gluino is significantly heavier than the QCD scale, Foster and Michael [46] were able to treat the gluino as a static particle, where the spin of the gluino is irrelevant so their results are applicable more generally to particles of arbitrary spin. If the static particle is sufficiently stable, then it will couple to surrounding gluons and quarks to form hadronic bound states. Foster and Michael used lattice QCD simulations to produce predictions for mass splittings within this new spectrum of hadrons. Specifically, Ref. [46] contains numerical results for two types of hadrons: gluelumps (having one static octet operator coupled to gluon fields, but no valence quarks) and adjoint mesons (having one static octet operator coupled to a quark-antiquark pair).

TABLE I: The smallest gluelump mass splittings relative to the 1^{+-} state from the original lattice simulation [46] (where errors are statistical only), compared to model calculations published subsequently. See Sec. III for a crucial discussion of lattice systematics. See the original publications for detailed discussions about other parameter choices and systematic issues; this table is merely an introduction. (To display data from Ref. [50] we chose $r_0 = 0.5$ fm.)

J^{PC}	$M(J^{PC}) - M(1^{+-})$ [GeV]				
	Lattice [46]	Bag [47]	String [48]	Coulomb gauge [49]	Transverse gluons [50]
1^{--}	0.368(7)	0.55	0.47	0.40	0.37
2^{--}	0.567(10) ^a	0.54	0.49	0.59	0.57
3^{+-}	0.972(24)	1.01	0.84	1.11	0.97
2^{+-}	0.973(36)	1.21	0.83	0.71	0.94
0^{++}	1.092(28)	~1.2	0.91

^aThis entry repairs a simple typo in column 4 of Table III in Ref. [46], as can be seen by comparing with column 3 of that same table and with Fig. 3 in Ref. [46].

According to Ref. [46], the lightest gluelump has $J^{PC} = 1^{+-}$. The predicted mass splittings of the five next-lightest gluelumps are shown in Table I. Four model calculations [47–50] are also shown in Table I for comparison. We display mass differences because these are what emerge directly from the lattice simulations, but in fact the absolute mass scale has been determined in Ref. [51] using a combination of effective field theory and related lattice QCD input. After fixing this absolute mass scale, Ref. [51] then takes the gluelump mass splittings directly from Ref. [46]. We point to potential NRQCD [52] as an example of an important theoretical development that has requested further lattice studies of gluelumps.

The authors of Ref. [46] expressed surprise at the heaviness of their 0^{++} state, and also at the degeneracy of 2^{+-} and 3^{+-} . Lattice simulations use irreducible representations Λ of the octahedral group rather than continuum angular momentum J , so, for example, a $J = 2$ state should appear for both $\Lambda = E$ and $\Lambda = T_2$, but Ref. [46] points out that E^{++} and T_2^{++} are not degenerate in their lattice data though the discrepancy is consistent with degeneracy in the continuum limit. Because of the computational expense, Ref. [46] made use of quenched lattices so the authors expect at least a 10% systematic error. The work also relied exclusively on operators built from square paths on the lattice which allows access to only half of the possible Λ^{PC} representations (i.e. 10 out of 20), leaving quantum numbers such as $J^{PC} = 0^{+-}$, 0^{-+} , 0^{--} , and 1^{++} unstudied.

In the present work, we extend the basis of operators to the complete set of Λ^{PC} options, and we use dynamical (unquenched) lattices. This provides an opportunity to revisit some of the surprises revealed by Foster and Michael in their seminal work, and to predict additional gluelump masses. We also develop operators for generalized gluelumps by replacing the static octet source with a static source having a larger color representation. To avoid the expense of lattice simulations with valence quarks, we choose representations that need only gluons to produce a color-singlet generalized gluelump. Specifically we choose dimensions 10, 27, 28, and 35. We reiterate that our numerical results make use of dynamical lattice simulations so that virtual quarks and antiquarks are retained.

Static propagators are known to produce particularly large statistical uncertainties in lattice simulations, and a static octet particle is noisier than a static triplet [46, 53]. We expect that the larger representations included in the present study will be noisier still. Also,

TABLE II: Young tableaux for representations relevant to this work. Labels inside boxes are to aid the discussion of (anti)symmetrization.

n_D	8	10	27	28	35
Tableau	$\begin{array}{ c c } \hline i & j \\ \hline k & \\ \hline \end{array}$	$\begin{array}{ c c c } \hline i & j & k \\ \hline & & \\ \hline \end{array}$	$\begin{array}{ c c c c } \hline i & j & k & l \\ \hline m & n & & \\ \hline \end{array}$	$\begin{array}{ c c c c c c } \hline i & j & k & l & m & n \\ \hline & & & & & \\ \hline \end{array}$	$\begin{array}{ c c c c c } \hline i & j & k & l & m \\ \hline n & & & & \\ \hline \end{array}$

the Casimir scaling hypothesis [54–56] is the notion that the string tension between strongly interacting particles should be proportional to the quadratic Casimir, and standard group theory [57, 58] shows that the quadratic Casimirs for our representations, normalized such that the triplet has $C_2(3) = 4/3$, are $C_2(8) = 3$, $C_2(10) = 6$, $C_2(27) = 8$, $C_2(28) = 18$, and $C_2(35) = 12$. Polyakov loops with all of these representations have been tested previously for Casimir scaling: see Table 2 of Ref. [59]. [For other lattice studies of Casimir scaling and various representations in four-dimensional SU(3) gauge theory, sometimes in the context of n -ality, see Refs. [60–69]. The present work deals exclusively with zero n -ality.] In the case of gluelumps, our simulations confirm that signals for representations with larger Casimirs are damped more rapidly as a function of Euclidean time, as well as being statistically noisy. Despite these substantial difficulties, the numerical results of this project provide useful information about representations beyond the octet, as well as the octet itself.

II. CORRELATION FUNCTIONS

Generalized gluelumps do not involve valence quarks, so the heavy static particle must be able to form a color singlet by coupling to a collection of octet gauge fields,

$$8 \otimes 8 \otimes 8 \otimes \dots \in 1 \oplus 8 \oplus 10 \oplus \overline{10} \oplus 27 \oplus 28 \oplus \overline{28} \oplus 35 \oplus \overline{35} \oplus \dots \quad (1)$$

Representations of dimension $n_D = 8, 10, 27, 28$, and 35 will be considered in this work. The corresponding Young tableaux, derivable using standard group theory methods [57, 58], are displayed in Table II. Notice that the number of boxes in each tableau is a multiple of 3, as required for tableaux built exclusively from octet gauge fields. As will be discussed below, each generalized gluelump will have a tensor where the number of indices equals the number of columns in its Young tableau.

As is standard in lattice QCD simulations, mass splittings will be obtained by computing a correlation function and then observing the exponential dependence on Euclidean time. A correlation function that creates a gluelump at Euclidean time τ_i and then annihilates it at time τ_f is

$$C(\tau_f - \tau_i) = H^{(n_D)\alpha\dagger}(\tau_i) G^{(n_D)\alpha\beta}(\tau_i, \tau_f) H^{(n_D)\beta}(\tau_f). \quad (2)$$

Repeated indices α and β are summed from 1 to n_D to produce a gauge-invariant correlation function. The operators H and H^\dagger that, respectively, annihilate and create the required gauge field structure will be developed in Sec. II B. The propagator G for the static particle is described presently.

A. Static propagator

A static particle propagates purely in the temporal direction (subscript “4”), so for a representation of dimension n_D we can write

$$G^{(n_D)\alpha\beta}(\tau_i, \tau_f) = U_4^{(n_D)\alpha\gamma}(\vec{x}, \tau_i) U_4^{(n_D)\gamma\delta}(\vec{x}, \tau_i + a) U_4^{(n_D)\delta\epsilon}(\vec{x}, \tau_i + 2a) \cdots U_4^{(n_D)\zeta\beta}(\vec{x}, \tau_f) \quad (3)$$

with repeated Greek indices summed from 1 to n_D . Each generalized link $U^{(n_D)}$ is built from elementary links (one per column of the Young tableau) contracted at each end (e.g. Euclidean times τ_i and $\tau_i + a$) with a basis tensor T ,

$$U^{(8)\alpha\beta} = U_{ik} U_{jl}^* T_{ij}^\alpha T_{kl}^\beta, \quad (4)$$

$$U^{(10)\alpha\beta} = U_{il} U_{jm} U_{kn} T_{ijk}^\alpha T_{lmn}^\beta, \quad (5)$$

$$U^{(27)\alpha\beta} = U_{im} U_{jn} U_{ko}^* U_{lp}^* T_{ijkl}^\alpha T_{mnop}^\beta, \quad (6)$$

$$U^{(28)\alpha\beta} = U_{io} U_{jp} U_{kq} U_{lr} U_{ms} U_{nt} T_{ijklmn}^\alpha T_{opqrst}^\beta, \quad (7)$$

$$U^{(35)\alpha\beta} = U_{in} U_{jo} U_{kp} U_{lq} U_{mr}^* T_{ijklm}^\alpha T_{nopqr}^\beta, \quad (8)$$

where repeated color indices i, j, k, \dots are summed from 1 to 3.

An acceptable basis for the octet representation is $T^\alpha = \lambda^\alpha / \sqrt{2}$ where λ^α is a standard Gell-Mann matrix as was used in Ref. [46]. Beyond the octet we find it more convenient to use real T tensors, and for consistency we will also use real matrices for the octet itself.

For a Young tableau with n_B boxes, we begin with an arbitrary tensor having n_B indices. Then we symmetrize all indices within a row. Next we antisymmetrize all indices within any column having two boxes and multiply that pair of indices by a Levi-Civita tensor, thus reducing the number of indices by one for each antisymmetrized column. The final step is to select a real basis of T tensors. For example, consider the 27-plet. An arbitrary 6-index tensor is a^{ijklmn} , and after symmetrization of (i, j, k, l) , symmetrization of (m, n) and then antisymmetrization of (i, m) and (j, n) , we have

$$b^{ijklmn} = a^{ijklmn} - a^{mjklin} - a^{inklmj} + a^{mnklij} + \dots \quad (9)$$

which reduces to a 4-index tensor,

$$T_{klpq} = \frac{1}{4} \epsilon_{imp} \epsilon_{jnq} b^{ijklmn}. \quad (10)$$

Evaluation of all $3^4 = 81$ elements of this tensor reveals that it contains 36 distinct entries but only 27 of them are linearly independent due to the following 9 constraints:

$$\begin{aligned} T_{1112} + T_{1222} + T_{1323} &= 0, \\ T_{1211} + T_{2212} + T_{2313} &= 0, \\ T_{1111} + T_{1212} + T_{1313} &= 0, \\ T_{1113} + T_{1333} + T_{1223} &= 0, \\ T_{2322} + T_{3323} + T_{1312} &= 0, \\ T_{2222} + T_{1212} + T_{2323} &= 0, \\ T_{2223} + T_{2333} + T_{1213} &= 0, \end{aligned}$$

$$\begin{aligned}
T_{3313} + T_{1311} + T_{2312} &= 0, \\
T_{3333} + T_{1313} + T_{2323} &= 0.
\end{aligned}
\tag{11}$$

Our choice for the basis of 27 tensors is given explicitly in Appendix A together with the other representations: octet, decuplet, 28-plet, and 35-plet.

As a useful check of these expressions, we calculate a completeness relation for each case: Appendix A verifies that the quantity

$$\sum_{\alpha=1}^{n_D} T^\alpha T^\alpha
\tag{12}$$

comprises a simple Kronecker delta structure. This is important for the gauge invariance of our correlation functions.

Notice also that our decuplet representation agrees with Appendix B of Ref. [70]. Finally, we mention that we have verified numerically that our real basis of octet T tensors produces correlation functions that are identical to those obtained in the Gell-Mann basis.

B. Creation/annihilation operators

The remaining ingredient needed for the computation of correlation functions is the set of operators, H of Eq. (2), coupling to the generalized gluelumps. An H operator is built from products of gauge links that join to the static particle propagator via a T tensor (from Sec. II A). Planar squares were used for H operators in Ref. [46], but this provides access to only half of the possible quantum numbers. Our most basic building block will be a “chair,” i.e. a 1×2 rectangle bent to a 90° angle, which provides access to all quantum numbers. For extra confirmation of numerics, we also ran simulations with the planar square operators used by Foster and Michael, and we verified that results are consistent with the corresponding chair-based operators defined here.

Figure 1 displays a pair of chairs touching each other at one lattice site and rotated into all of the 24 orientations that are possible on a cubic lattice. Notice that each chair has a particular direction because a “backward link” $U_{-\mu}(x + \mu) = U_\mu^\dagger(x)$ is not equal to the “forward link” $U_\mu(x)$. Within each pair of chairs in Fig. 1, $A + B$ is a positive parity operator and $A - B$ is a negative parity operator. Because $U_\mu(x) \rightarrow U_\mu^\dagger(x)$ under charge conjugation, a “forward” chair plus a “backwards” chair has positive charge conjugation and the difference between these two chairs has negative charge conjugation.

The five bosonic irreducible representations of the octahedral group are $\Lambda = A_1, A_2, T_1, T_2,$ and E , and their smallest continuum angular momenta are $J = 0, 3, 1, 2,$ and 2 , respectively. For octet gluelumps, the corresponding operators are obtained from specific linear combinations of the chair-shaped paths in Fig. 1. The steps of a derivation are provided in Appendix B, and the results are given here:

$$\begin{aligned}
H^{(8)\alpha}(A_1) &= \left(\sum_{a=1}^{24} L_a^{(8)} \right)_{ij} T_{ij}^\alpha, \\
H^{(8)\alpha}(A_2) &= \left(\sum_{a=1}^{12} (-1)^a L_a^{(8)} - \sum_{a=13}^{24} (-1)^a L_a^{(8)} \right)_{ij} T_{ij}^\alpha,
\end{aligned}$$

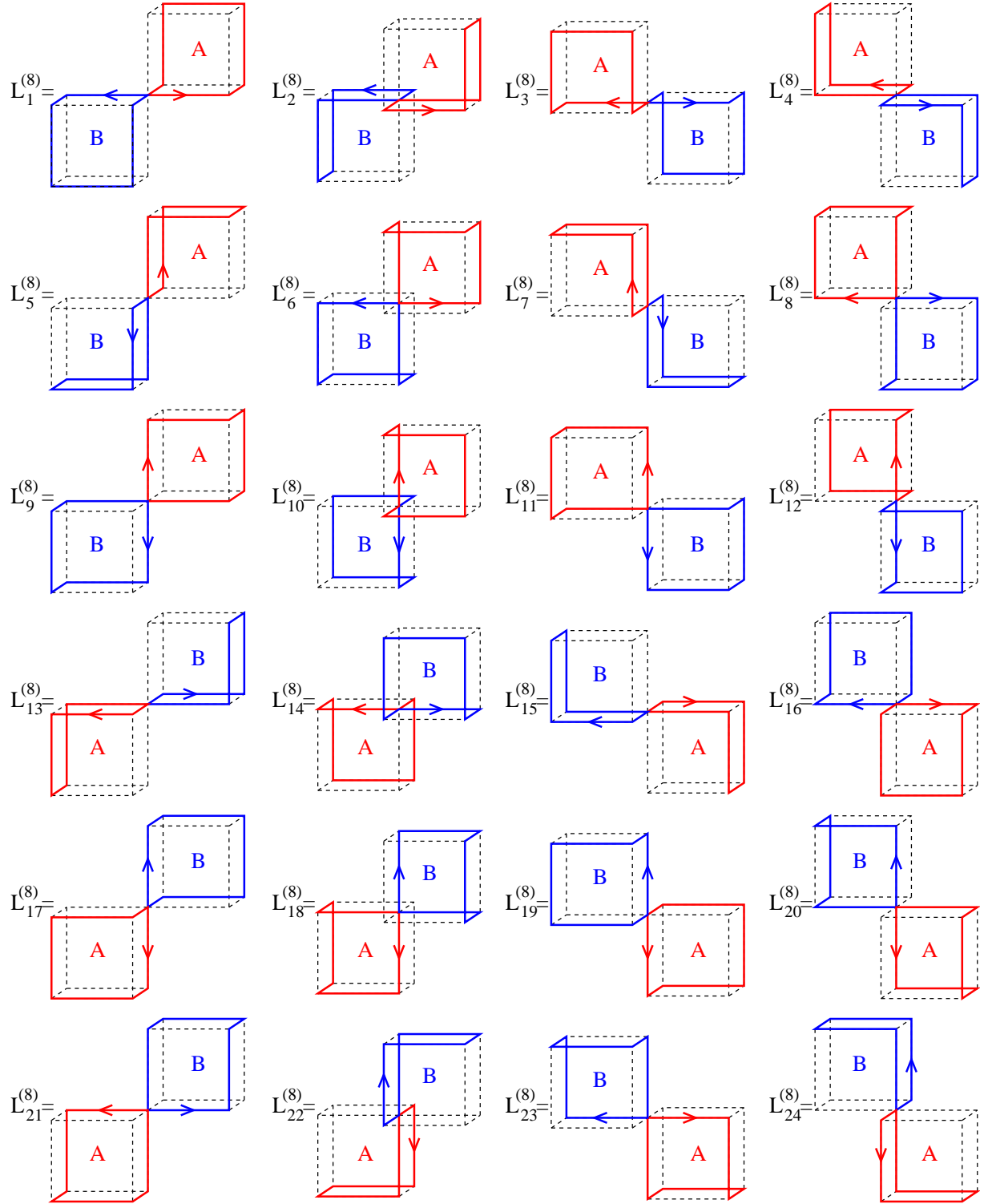


FIG. 1: Each chair-shaped path is the product of six gauge links used to build operators for octet gluelumps. Solid lines are the gauge links; dashed lines are just to aid with three-dimensional (3D) visualization.

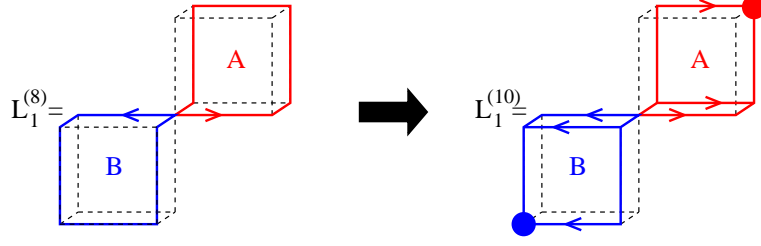


FIG. 2: Octet chairs and decuplet chairs have the same shape but the product of gauge links differs. Solid lines are the gauge links; dashed lines are just to aid with 3D visualization. A filled circle denotes insertion of a Levi-Civita tensor.

$$\begin{aligned}
H^{(8)\alpha}(T_1^x) &= \left(L_6^{(8)} + L_{20}^{(8)} + L_{21}^{(8)} + L_{11}^{(8)} - L_{18}^{(8)} - L_8^{(8)} - L_9^{(8)} - L_{23}^{(8)} \right)_{ij} T_{ij}^\alpha, \\
H^{(8)\alpha}(T_1^y) &= \left(L_5^{(8)} + L_{19}^{(8)} + L_{24}^{(8)} + L_{10}^{(8)} - L_{17}^{(8)} - L_7^{(8)} - L_{12}^{(8)} - L_{22}^{(8)} \right)_{ij} T_{ij}^\alpha, \\
H^{(8)\alpha}(T_1^z) &= \left(L_1^{(8)} + L_2^{(8)} + L_3^{(8)} + L_4^{(8)} - L_{13}^{(8)} - L_{14}^{(8)} - L_{15}^{(8)} - L_{16}^{(8)} \right)_{ij} T_{ij}^\alpha, \\
H^{(8)\alpha}(T_2^x) &= \left(L_6^{(8)} - L_{20}^{(8)} + L_{21}^{(8)} - L_{11}^{(8)} + L_{18}^{(8)} - L_8^{(8)} + L_9^{(8)} - L_{23}^{(8)} \right)_{ij} T_{ij}^\alpha, \\
H^{(8)\alpha}(T_2^y) &= \left(L_5^{(8)} - L_{19}^{(8)} + L_{24}^{(8)} - L_{10}^{(8)} + L_{17}^{(8)} - L_7^{(8)} + L_{12}^{(8)} - L_{22}^{(8)} \right)_{ij} T_{ij}^\alpha, \\
H^{(8)\alpha}(T_2^z) &= \left(L_1^{(8)} - L_2^{(8)} + L_3^{(8)} - L_4^{(8)} + L_{13}^{(8)} - L_{14}^{(8)} + L_{15}^{(8)} - L_{16}^{(8)} \right)_{ij} T_{ij}^\alpha, \\
H^{(8)\alpha}(E^1) &= (v^x - v^y)_{ij} T_{ij}^\alpha, \\
H^{(8)\alpha}(E^2) &= (v^x + v^y - 2v^z)_{ij} T_{ij}^\alpha, \\
v^x &= L_6^{(8)} + L_{20}^{(8)} + L_{21}^{(8)} + L_{11}^{(8)} + L_{18}^{(8)} + L_8^{(8)} + L_9^{(8)} + L_{23}^{(8)}, \\
v^y &= L_5^{(8)} + L_{19}^{(8)} + L_{24}^{(8)} + L_{10}^{(8)} + L_{17}^{(8)} + L_7^{(8)} + L_{12}^{(8)} + L_{22}^{(8)}, \\
v^z &= L_1^{(8)} + L_2^{(8)} + L_3^{(8)} + L_4^{(8)} + L_{13}^{(8)} + L_{14}^{(8)} + L_{15}^{(8)} + L_{16}^{(8)}. \tag{13}
\end{aligned}$$

Notice that A_1 and A_2 are one-dimensional representations, T_1 and T_2 are three dimensional, and E is two dimensional.

Each decuplet chair contains three paths that begin at a central lattice site (where the tensor T will be placed) and end at a Levi-Civita tensor. Each of those three paths is the product of three gauge links. The precise definition of $L_1^{(10)}$ is displayed in Fig. 2, and $L_2^{(10)}$ through $L_{24}^{(10)}$ are defined by applying the same procedure to every chair in Fig. 1. The decuplet operators are obtained by making two simple adjustments to Eqs. (13): replace every superscript (8) with a superscript (10) and replace every pair of indices ij by the three indices ijk .

The 35-plet is built from a double chair, specifically one octet-type chair and one decuplet-type chair, defined as follows:

$$\begin{aligned}
\left(L_1^{(35)} \right)_{ijklm} &= \left(L_5^{(8)} \right)_{im} \left(L_9^{(10)} \right)_{jkl}, & \left(L_{13}^{(35)} \right)_{ijklm} &= \left(L_{21}^{(8)} \right)_{im} \left(L_{17}^{(10)} \right)_{jkl}, \\
\left(L_2^{(35)} \right)_{ijklm} &= \left(L_6^{(8)} \right)_{im} \left(L_{10}^{(10)} \right)_{jkl}, & \left(L_{14}^{(35)} \right)_{ijklm} &= \left(L_{22}^{(8)} \right)_{im} \left(L_{18}^{(10)} \right)_{jkl},
\end{aligned}$$

$$\begin{aligned}
\left(L_3^{(35)}\right)_{ijklm} &= \left(L_7^{(8)}\right)_{im} \left(L_{11}^{(10)}\right)_{jkl}, & \left(L_{15}^{(35)}\right)_{ijklm} &= \left(L_{23}^{(8)}\right)_{im} \left(L_{19}^{(10)}\right)_{jkl}, \\
\left(L_4^{(35)}\right)_{ijklm} &= \left(L_8^{(8)}\right)_{im} \left(L_{12}^{(10)}\right)_{jkl}, & \left(L_{16}^{(35)}\right)_{ijklm} &= \left(L_{24}^{(8)}\right)_{im} \left(L_{20}^{(10)}\right)_{jkl}, \\
\left(L_5^{(35)}\right)_{ijklm} &= \left(L_9^{(8)}\right)_{im} \left(L_1^{(10)}\right)_{jkl}, & \left(L_{17}^{(35)}\right)_{ijklm} &= \left(L_{13}^{(8)}\right)_{im} \left(L_{21}^{(10)}\right)_{jkl}, \\
\left(L_6^{(35)}\right)_{ijklm} &= \left(L_{10}^{(8)}\right)_{im} \left(L_2^{(10)}\right)_{jkl}, & \left(L_{18}^{(35)}\right)_{ijklm} &= \left(L_{14}^{(8)}\right)_{im} \left(L_{22}^{(10)}\right)_{jkl}, \\
\left(L_7^{(35)}\right)_{ijklm} &= \left(L_{11}^{(8)}\right)_{im} \left(L_3^{(10)}\right)_{jkl}, & \left(L_{19}^{(35)}\right)_{ijklm} &= \left(L_{15}^{(8)}\right)_{im} \left(L_{23}^{(10)}\right)_{jkl}, \\
\left(L_8^{(35)}\right)_{ijklm} &= \left(L_{12}^{(8)}\right)_{im} \left(L_4^{(10)}\right)_{jkl}, & \left(L_{20}^{(35)}\right)_{ijklm} &= \left(L_{16}^{(8)}\right)_{im} \left(L_{24}^{(10)}\right)_{jkl}, \\
\left(L_9^{(35)}\right)_{ijklm} &= \left(L_1^{(8)}\right)_{im} \left(L_5^{(10)}\right)_{jkl}, & \left(L_{21}^{(35)}\right)_{ijklm} &= \left(L_{17}^{(8)}\right)_{im} \left(L_{13}^{(10)}\right)_{jkl}, \\
\left(L_{10}^{(35)}\right)_{ijklm} &= \left(L_2^{(8)}\right)_{im} \left(L_6^{(10)}\right)_{jkl}, & \left(L_{22}^{(35)}\right)_{ijklm} &= \left(L_{18}^{(8)}\right)_{im} \left(L_{14}^{(10)}\right)_{jkl}, \\
\left(L_{11}^{(35)}\right)_{ijklm} &= \left(L_3^{(8)}\right)_{im} \left(L_7^{(10)}\right)_{jkl}, & \left(L_{23}^{(35)}\right)_{ijklm} &= \left(L_{19}^{(8)}\right)_{im} \left(L_{15}^{(10)}\right)_{jkl}, \\
\left(L_{12}^{(35)}\right)_{ijklm} &= \left(L_4^{(8)}\right)_{im} \left(L_8^{(10)}\right)_{jkl}, & \left(L_{24}^{(35)}\right)_{ijklm} &= \left(L_{20}^{(8)}\right)_{im} \left(L_{16}^{(10)}\right)_{jkl}. \quad (14)
\end{aligned}$$

Notice that a diagram of $L_n^{(35)}$ would resemble $L_n^{(8)}$ of Fig. 1 except that the chairs in each lattice cell are in the opposite locations (there *is* a chair where there *was not*, and there *is not* a chair where there *was*). There are two options—the octet-type chair could have been to the left or to the right of the decuplet-type chair when viewed from a certain angle—and Eqs. (14) show which of the two options we have selected. The 35-plet operators are obtained by making two simple adjustments to Eqs. (13): replace every superscript (8) with a superscript (35) and replace every pair of indices ij by the set $ijklm$.

The 27-plet is also built from a double chair, but both are octet-type chairs. The definition is obtained from Eqs. (14) with these replacements: (35) \rightarrow (27), (10) \rightarrow (8), $ijklm \rightarrow ijkl$, $im \rightarrow ik$, $jkl \rightarrow jl$. The 27-plet operators are obtained by making two simple adjustments to Eqs. (13): replace every superscript (8) with a superscript (27) and replace every pair of indices ij by the set $ijkl$.

The 28-plet is built from a double chair; both are decuplet-type. The definition is obtained from Eqs. (14) with these replacements: (35) \rightarrow (28), (8) \rightarrow (10), $ijklm \rightarrow ijklmn$, $im \rightarrow ijk$, $jkl \rightarrow lmn$. The 28-plet operators are obtained by making two simple adjustments to Eqs. (13): replace every superscript (8) with a superscript (28) and replace every pair of indices ij by the set $ijklmn$.

To complete the discussion of generalized gluelump operators, notice that the octet and 27-plet are eigenstates of charge conjugation, whereas the decuplet, 28-plet, and 35-plet are not. This is evident from the Young tableaux representations of the underlying group theory as shown in Table II. Representations with twice as many boxes in the top row as the bottom row have the same number of symmetric and antisymmetric indices. They are their own antirepresentations and are eigenstates of charge conjugation. Other representations are “charged” and cannot form states with definite charge conjugation. This property can also be seen in the color flow in Figs. 1 and 2. Any single octet chair has one color and one anticolor emanating from the central lattice site, but the decuplet has three colors and no anticolors.

TABLE III: Input parameters and standard output parameters (separated by a horizontal line) used in this work were obtained from Ref. [71]. For comparison, parameters used in the quenched study by Ref. [46] are also shown.

Source	[71]	[71]	[46]	[46]	[46]
β	1.90	2.05	5.7	6.0	6.2
κ_{ud}	0.13700	0.13560
κ_s	0.13640	0.13540
c_{SW}	1.7150	1.6280
$L^3 \times T$	$20^3 \times 40$	$28^3 \times 56$	$12^3 \times 24$	$16^3 \times 48$	$24^3 \times 48$
No. of configurations	790	650	99	202	60
Lattice spacing [fm]	0.0982(19)	0.0685(26)	0.170	0.0948	0.0683
m_π/m_ρ	0.6243(28)	0.6361(47)
$\sqrt{2m_K^2 - m_\pi^2}/m_\phi$	0.7102(20)	0.6852(46)

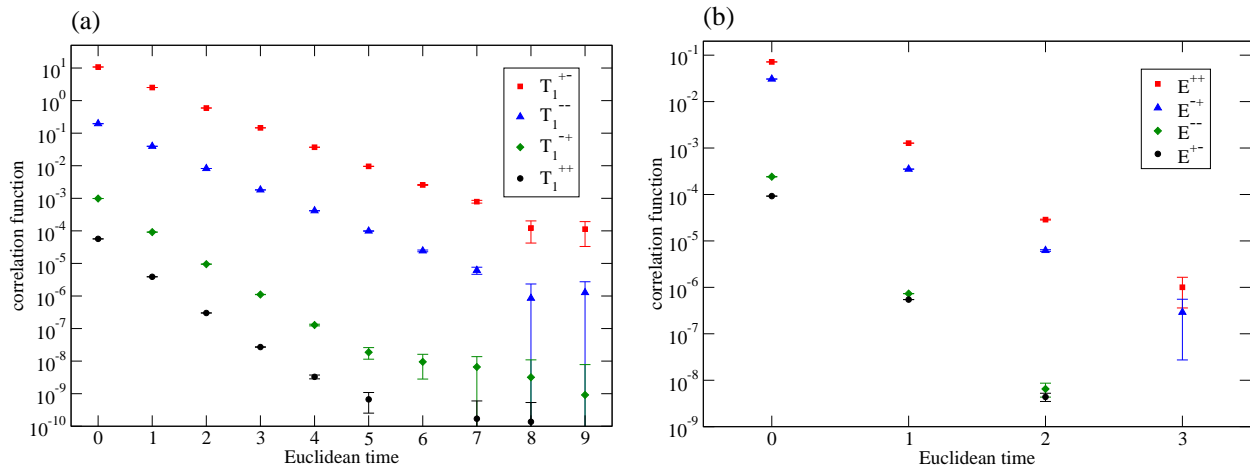


FIG. 3: Sample correlation functions: (a) the T_1^{PC} channels containing a static octet particle at $\beta = 2.05$, (b) the E^{PC} channels containing a static 27-plet particle at $\beta = 1.90$.

III. LATTICE SIMULATIONS

The simulations performed for this work use two ensembles of configurations provided by the CP-PACS and JLQCD Collaborations [71]. These ensembles are $O(a)$ -improved due to the use of the clover coefficient, c_{SW} . The lattice spacings are comparable to the smallest values used in Ref. [46]. Precise parameter values are displayed in Table III. Notice that the strange quark mass is essentially its physical value, but the up and down quarks are not: the pion is about 3.5 times heavier than its physical value.

Stout link smearing [72] was applied to the operators of Sec. II B with parameters tuned to reduce contamination from excited states. In the notation of Ref. [72], we use $(\rho, n_\rho) = (0.20, 15)$ for the octet and decuplet, and we use $(\rho, n_\rho) = (0.15, 15)$ for the 27-plet, 28-plet, and 35-plet. Figure 3 gives an indication of the quality of the data by showing the relatively clean example of the octet T_1^{PC} as well as the much more challenging example of the 27-plet E^{PC} .

TABLE IV: The mass spectrum of gluelumps containing a static octet particle, as determined from dynamical lattice QCD at two lattice spacings. J denotes the continuum angular momentum of the light (gauge) degrees of freedom and does not include the spin of the octet particle. The first error is statistical and the second is systematic, from Eq. (16).

Λ^{PC}	J	$M(\Lambda^{PC}) - M(T_1^{+-})$ [GeV]	
		$\beta = 1.90$	$\beta = 2.05$
T_1^{--}	1	$0.33 \pm 0.02 \pm 0.07$	$0.24 \pm 0.05 \pm 0.06$
E^{--}	2	$0.66 \pm 0.02 \pm 0.07$	$0.87 \pm 0.04 \pm 0.05$
T_2^{--}	2	$0.67 \pm 0.02 \pm 0.06$	$0.64 \pm 0.11 \pm 0.09$
E^{+-}	2	$0.94 \pm 0.03 \pm 0.08$	$1.18 \pm 0.05 \pm 0.06$
T_2^{+-}	2	$1.12 \pm 0.03 \pm 0.08$	$1.39 \pm 0.06 \pm 0.06$
A_1^{++}	0	$1.14 \pm 0.05 \pm 0.11$	$1.55 \pm 0.12 \pm 0.09$
A_2^{+-}	3	$1.39 \pm 0.12 \pm 0.22$	$2.27 \pm 0.05 \pm 0.25$
A_1^{--}	0	$1.44 \pm 0.09 \pm 0.19$	$1.73 \pm 0.23 \pm 0.26$
E^{++}	2	$1.51 \pm 0.07 \pm 0.11$	$2.07 \pm 0.03 \pm 0.15$
T_2^{++}	2	$2.00 \pm 0.13 \pm 0.13$	$2.88 \pm 0.05 \pm 0.18$
T_1^{++}	1	$2.14 \pm 0.15 \pm 0.19$	$2.14 \pm 0.38 \pm 0.45$
T_1^{-+}	1	$1.59 \pm 0.06 \pm 0.12$	$2.31 \pm 0.04 \pm 0.16$
A_2^{-+}	3	$1.71 \pm 0.14 \pm 0.24$	$2.54 \pm 0.06 \pm 0.23$
E^{-+}	2	$1.89 \pm 0.10 \pm 0.06$	$2.45 \pm 0.04 \pm 0.16$
T_2^{-+}	2	$1.86 \pm 0.09 \pm 0.11$	$2.52 \pm 0.04 \pm 0.19$
A_2^{++}	3	$1.91 \pm 0.33 \pm 0.42$	$3.20 \pm 0.12 \pm 0.29$
A_2^{--}	3	$2.97 \pm 0.05 \pm 0.59$	$3.58 \pm 0.19 \pm 0.32$
A_1^{-+}	0	$3.02 \pm 0.05 \pm 0.48$	$3.82 \pm 0.18 \pm 0.17$
A_1^{+-}	0	$2.82 \pm 0.04 \pm 0.41$	$3.44 \pm 0.13 \pm 0.19$

Mass differences are obtained by the simultaneous fit of a pair of correlation functions:

$$C_1 = f_1 e^{-M_1 \tau} \quad \text{and} \quad C_2 = f_2 e^{-(M_1 + \delta M_{12}) \tau} \quad (15)$$

where f_1 , f_2 , M_1 , and δM_{12} are the four fit parameters. The mass difference δM_{12} is the physics we wish to extract, and its statistical uncertainty is determined by bootstrapping [73]. The most important systematic uncertainty comes from choosing the range of time steps, τ_i to τ_f , to include in each fit. Fits do not depend significantly on τ_f because the inclusion of noisy data at large Euclidean times has a negligible influence. We determined the range of τ_i options that all produced a common δM_{12} value within one statistical standard deviation, and then used the smallest τ_i in that range because it produces the smallest statistical uncertainty. A one-sigma systematic error was then assigned to be

$$\left| \frac{\delta M_{12}(\tau_i) - \delta M_{12}(\tau_i - 1)}{2} \right|. \quad (16)$$

Table IV and Fig. 4 contain the final results for mass splittings among gluelumps with the static particle in the color-octet representation. As is true throughout this article, angular momentum J refers to the light degrees of freedom only; all results apply to a heavy

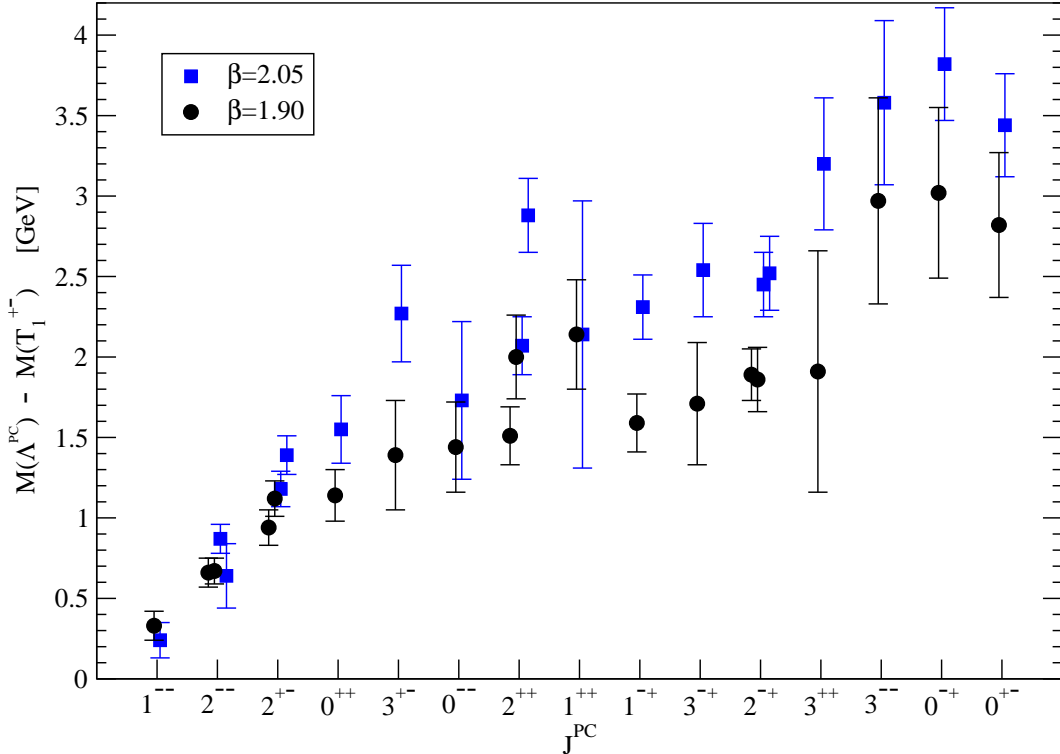


FIG. 4: The content of Table IV is displayed visually. Statistical and systematic errors were added linearly.

particle—color octet in this case—with *any* spin. Although the central value for the mass difference at $\beta = 2.05$ tends to be larger than the central value at $\beta = 1.90$, the effect is marginal relative to the quoted error bars. Since both lattice spacings are less than 0.1 fm and an improved lattice QCD action has been used, it is not surprising that mass splittings are essentially independent of lattice spacing. It is also reassuring to see that E^{PC} and T_2^{PC} are consistent with each other for each PC , since they should couple to the same physical state ($J = 2$) in the continuum limit.

The quenched lattice QCD study of Ref. [46] had access to only 10 of the 20 channels listed in our Table IV. The raw data for those 10 channels are provided in Table II of Ref. [46] (here called “[46]-II” for brevity) without systematic errors, but several options for adjacent time steps are shown in [46]-II and from this a systematic error defined by our Eq. (16) can be estimated if desired. The raw data from [46]-II are in reasonable agreement with the present work, but we wish to point out some concerns about how [46]-II was used to arrive at final mass splittings in MeV, as listed in [46]-III.

To begin, we note that [46]-III was obtained from [46]-II by going through the figure [46]-3. The figure [46]-3 is largely obtained from [46]-II by using the first two time steps (called “ $t=2:1$ ” in Ref. [46]) and combining errors from the two energy levels in quadrature. This numerically reproduces the data in [46]-3 with two exceptions, both at $\beta = 5.7$: the A_1^{++} data point in [46]-3 is not consistent with [46]-II, and neither is the error bar for T_2^{++} . A first concern is that $\beta = 5.7$ data have a significant impact on the continuum extrapolation presented in [46]-III, and direct use of [46]-II indicates a much more modest lattice spacing dependence than was claimed. A second concern is that the $t=2:1$ data are used to obtain

TABLE V: The mass spectrum of gluelumps containing a static decuplet particle, as determined from dynamical lattice QCD at $\beta = 1.90$. J denotes the continuum angular momentum of the light (gauge) degrees of freedom and does not include the spin of the decuplet particle. The first error is statistical and the second is systematic, from Eq. (16).

Λ^P	J	$M(\Lambda^P) - M(A_1^-)$ [GeV]
T_1^-	1	$0.39 \pm 0.04 \pm 0.33$
E^-	2	$0.40 \pm 0.05 \pm 0.33$
T_2^-	2	$0.41 \pm 0.04 \pm 0.32$
T_1^+	1	$0.57 \pm 0.05 \pm 0.48$
A_2^+	3	$0.89 \pm 0.10 \pm 0.47$
E^+	2	$0.90 \pm 0.07 \pm 0.45$
T_2^+	2	$0.96 \pm 0.06 \pm 0.37$
A_1^+	0	$1.05 \pm 0.10 \pm 0.38$
A_2^-	3	$1.48 \pm 0.17 \pm 0.44$

the continuum limit even though [46]-II shows that they produce mass splittings that differ significantly from later time steps.

These concerns should not detract from the valuable comparison between the present study and [46]-II. Our dynamical lattice QCD study uses two lattice spacings that are very close to the finer two spacings of the quenched study in Ref. [46], and produces compatible results, which indicates that quenching errors are too small to disentangle from the other uncertainties. The authors of Ref. [46] reported a lack of degeneracy for E^{++} and T_2^{++} at nonzero lattice spacings, with T_2^{++} heavier than E^{++} , and we see a similar tendency though it is not large relative to the error bars in Fig. 4. Moreover, we now have three other channels ($+-$, $-+$, and $--$) where E and T_2 can be compared, and these are all appropriately degenerate when systematic uncertainties are taken into account. The authors of Ref. [46] were surprised by the degeneracy of 2^{+-} with 3^{+-} , but in the context of our 20-channel study this pair of operators has no striking degeneracy. The authors of Ref. [46] were surprised by the heaviness of the 0^{++} , and we agree that it is heavy, although the extrapolation in Ref. [46] is noticeably reduced when the $\beta = 5.7$ data are taken directly from [46]-II.

For representations beyond the octet, our efforts to optimize the smeared operators were concentrated on the $\beta = 1.90$ ensemble. Simulations of the $\beta = 2.05$ lattices were computationally expensive and, like the octet results, we do not anticipate a significant dependence on lattice spacing between these two β values, so our results at $\beta = 1.90$ represent predictions for the continuum physics spectrum. Mass splittings for gluelumps with the static particle in the color-decuplet representation are shown in Table V. Notice that the A_1^- , which in the continuum is 0^- , appears to be the lightest state in this spectrum modulo systematic uncertainties.

Mass splittings for gluelumps containing a 27-plet static particle are shown in Table VI. All 20 Λ^{PC} channels were attempted, but those omitted from the table produced no usable signal. Although mass differences are tabulated relative to T_2^{++} , the data do not ensure that this is the lightest state. For both the decuplet and the 27-plet, the E and T_2 channels are consistent with one another.

Correlation functions for the 28-plet and 35-plet contained too few usable time steps to give a meaningful systematic error, so we refrain from presenting numerical results. Never-

TABLE VI: The resolvable mass spectrum of gluelumps containing a static 27-plet particle, as determined from dynamical lattice QCD at $\beta = 1.90$. J denotes the continuum angular momentum of the light (gauge) degrees of freedom and does not include the spin of the 27-plet particle. The first error is statistical and the second is systematic, from Eq. (16).

Λ^{PC}	J	$M(\Lambda^{PC}) - M(T_2^{++})$ [GeV]
E^{++}	2	$0.04 \pm 0.06 \pm 0.24$
A_1^{++}	0	$0.05 \pm 0.07 \pm 0.19$
T_2^{-+}	2	$0.50 \pm 0.08 \pm 0.45$
E^{-+}	2	$0.53 \pm 0.09 \pm 0.43$
T_1^{-+}	1	$0.66 \pm 0.09 \pm 0.38$
A_2^{-+}	3	$0.74 \pm 0.17 \pm 0.50$
A_2^{++}	3	$1.12 \pm 0.23 \pm 0.45$
T_1^{+-}	1	$1.29 \pm 0.26 \pm 0.93$
T_1^{++}	1	$1.34 \pm 0.20 \pm 0.57$
T_2^{+-}	2	$1.91 \pm 0.32 \pm 0.45$
E^{+-}	2	$2.13 \pm 0.41 \pm 0.30$
T_1^{--}	1	$2.49 \pm 0.55 \pm 0.44$

theless, the writing and running of this code helped us to confirm the operator definitions presented in Secs. II A and II B and Appendixes A and B—for example, we tested gauge invariance through explicit computations with a single configuration in every case.

Although none of the operators used in the present work contain valence quarks, physical states with valence quarks could have the same quantum numbers as gluelumps. Examples of such states include the adjoint mesons in Ref. [46] that were explored on quenched lattices by using operators that contain explicit valence quarks. As exemplified by Fig. 8 of Ref. [46], the mass difference between gluelumps and adjoint mesons is difficult to ascertain. Our use of dynamical configurations in principle allows adjoint mesons to mix with the gluelump signals, but our exclusive use of quark-free operators likely produces only a feeble coupling to adjoint mesons. A combined study of adjoint mesons and gluelumps would require operators of both types to be analyzed simultaneously in a matrix that permits mixing between them.

IV. CONCLUSIONS

Any extension of the standard model with a long-lived colored heavy particle will contain new hadrons that are QCD bound states of the heavy particle together with gluons and quarks. The lattice QCD study of this new hadron spectrum was pioneered by Michael and collaborators [43–46], motivated by the color-octet gluino of supersymmetry.

The present study has revisited the gluelump spectrum in greater detail. This is the first lattice simulation to explore the complete set of gluelump quantum numbers, J^{PC} , where J represents the angular momentum of the light degrees of freedom. The heavy particle is treated as static, so its spin decouples. The lightest new state not studied previously is 0^{--} , which is found to be as light as some of the states that were studied in Ref. [46]. Comparison of E and T_2 representations, both of which couple to $J = 2$ in the continuum limit, provides a cross-check on systematic errors. A leading systematic error was identified as arising from

the choice of a fitting window in Euclidean time. Comparison of the quenched results from Ref. [46] with the present dynamical results does not reveal any large quenching artifacts.

In addition, the present study provides the first results for generalized gluelumps, where the heavy particle is not color octet but rather decuplet or 27-plet. The machinery for 28-plet and 35-plet computations was also established and tested, so future studies will be straightforward in those cases as well.

Final numerical results are presented in Tables IV, V, and VI. The two β values for octet results represent two different lattice spacings that agree within uncertainties. Comparison of Table IV with the previous studies tabulated in Table I shows a general agreement, and indicates that systematic errors cannot be neglected: lattice results are presently limited by systematics rather than statistics. Future studies can directly use the operators developed here to perform larger-scale simulations and improve the precision for this spectrum of generalized gluelumps.

Acknowledgments

We thank the CP-PACS and JLQCD Collaborations for making their dynamical gauge field configurations available. This work was supported in part by the Natural Sciences and Engineering Research Council (NSERC) of Canada and by Compute Canada through the Shared Hierarchical Academic Research Computing Network (SHARCNET).

Appendix A: BASIS TENSORS FOR EACH REPRESENTATION

To reduce notational clutter, define generalized Kronecker delta functions where indices in parenthesis are to be permuted through all distinct orderings. A few examples are the following:

$$\begin{aligned}
\delta_{\{ij\}\{kk\}} &= \delta_{ik}\delta_{jk}, \\
\delta_{\{ij\}\{kl\}} &= \delta_{ik}\delta_{jl} + \delta_{il}\delta_{jk}, \\
\delta_{\{ijk\}\{lll\}} &= \delta_{il}\delta_{jl}\delta_{kl}, \\
\delta_{\{ijk\}\{llm\}} &= \delta_{il}\delta_{jl}\delta_{km} + \delta_{il}\delta_{jm}\delta_{kl} + \delta_{im}\delta_{jl}\delta_{kl}, \\
\delta_{\{ijk\}\{lmn\}} &= \delta_{il}\delta_{jm}\delta_{kn} + \delta_{il}\delta_{jn}\delta_{km} + \delta_{im}\delta_{jl}\delta_{kn} + \delta_{im}\delta_{jn}\delta_{kl} + \delta_{in}\delta_{jl}\delta_{km} + \delta_{in}\delta_{jm}\delta_{kl}, \\
\delta_{\{ijkl\}\{pppp\}} &= \delta_{ip}\delta_{jp}\delta_{kp}\delta_{lp}, \\
\delta_{\{ijkl\}\{pppq\}} &= \delta_{ip}\delta_{jp}\delta_{kp}\delta_{lq} + \delta_{ip}\delta_{jp}\delta_{kq}\delta_{lp} + \delta_{ip}\delta_{jq}\delta_{kp}\delta_{lp} + \delta_{iq}\delta_{jp}\delta_{kp}\delta_{lp}, \\
\delta_{\{ijkl\}\{ppqq\}} &= \delta_{ip}\delta_{jp}\delta_{kq}\delta_{lq} + \delta_{ip}\delta_{jq}\delta_{kp}\delta_{lq} + \delta_{iq}\delta_{jp}\delta_{kp}\delta_{lq} \\
&\quad + \delta_{ip}\delta_{jq}\delta_{kq}\delta_{lp} + \delta_{iq}\delta_{jp}\delta_{kq}\delta_{lp} + \delta_{iq}\delta_{jq}\delta_{kp}\delta_{lp}, \\
\delta_{\{ijkl\}\{ppqr\}} &= \delta_{ip}\delta_{jp}\delta_{kq}\delta_{lr} + \delta_{ip}\delta_{jq}\delta_{kp}\delta_{lr} + \delta_{iq}\delta_{jp}\delta_{kp}\delta_{lr} \\
&\quad + \delta_{ip}\delta_{jq}\delta_{kr}\delta_{lp} + \delta_{iq}\delta_{jp}\delta_{kr}\delta_{lp} + \delta_{iq}\delta_{jr}\delta_{kp}\delta_{lp} \\
&\quad + \delta_{ip}\delta_{jp}\delta_{kr}\delta_{lq} + \delta_{ip}\delta_{jr}\delta_{kp}\delta_{lq} + \delta_{ir}\delta_{jp}\delta_{kp}\delta_{lq} \\
&\quad + \delta_{ip}\delta_{jr}\delta_{kq}\delta_{lp} + \delta_{ir}\delta_{jp}\delta_{kq}\delta_{lp} + \delta_{ir}\delta_{jq}\delta_{kp}\delta_{lp}.
\end{aligned} \tag{A1}$$

The basis used for the octet representation is

$$\begin{aligned}
T_{ij}^1 &= \delta_{i1}\delta_{j2}, & T_{ij}^2 &= \delta_{i1}\delta_{j3}, & T_{ij}^3 &= \delta_{i2}\delta_{j3}, \\
T_{ij}^4 &= \delta_{i2}\delta_{j1}, & T_{ij}^5 &= \delta_{i3}\delta_{j1}, & T_{ij}^6 &= \delta_{i3}\delta_{j2}, \\
T_{ij}^7 &= \frac{1}{2}(\delta_{i1}\delta_{j1} - \delta_{i2}\delta_{j2}), & T_{ij}^8 &= \frac{1}{\sqrt{6}}(\delta_{i1}\delta_{j1} + \delta_{i2}\delta_{j2} - 2\delta_{i3}\delta_{j3}).
\end{aligned} \tag{A2}$$

The octet tensors obey the relation

$$\sum_{\mu=1}^8 T_{ij}^{\mu} T_{kl}^{\mu} = \delta_{ik}\delta_{jl} - \frac{1}{3}\delta_{ij}\delta_{kl}. \tag{A3}$$

The basis used for the decuplet representation is

$$\begin{aligned}
T_{ijk}^1 &= \delta_{\{ijk\}\{111\}}, & T_{ijk}^2 &= \delta_{\{ijk\}\{222\}}, & T_{ijk}^3 &= \delta_{\{ijk\}\{333\}}, \\
T_{ijk}^4 &= \frac{1}{\sqrt{3}}\delta_{\{ijk\}\{112\}}, & T_{ijk}^5 &= \frac{1}{\sqrt{3}}\delta_{\{ijk\}\{113\}}, & T_{ijk}^6 &= \frac{1}{\sqrt{3}}\delta_{\{ijk\}\{122\}}, \\
T_{ijk}^7 &= \frac{1}{\sqrt{3}}\delta_{\{ijk\}\{223\}}, & T_{ijk}^8 &= \frac{1}{\sqrt{3}}\delta_{\{ijk\}\{133\}}, & T_{ijk}^9 &= \frac{1}{\sqrt{3}}\delta_{\{ijk\}\{233\}}, \\
T_{ijk}^{10} &= \frac{1}{\sqrt{6}}\delta_{\{ijk\}\{123\}}.
\end{aligned} \tag{A4}$$

The decuplet tensors obey the relation

$$\sum_{\mu=1}^{10} T_{ijk}^{\mu} T_{lmn}^{\mu} = \frac{1}{6}\delta_{\{ijk\}}\delta_{\{lmn\}}. \tag{A5}$$

The basis used for the 27-plet representation is

$$\begin{aligned}
T_{ijkl}^1 &= \delta_{\{ij\}\{11\}}\delta_{\{kl\}\{22\}}, & T_{ijkl}^2 &= \delta_{\{ij\}\{11\}}\delta_{\{kl\}\{33\}}, & T_{ijkl}^3 &= \delta_{\{ij\}\{22\}}\delta_{\{kl\}\{33\}}, \\
T_{ijkl}^4 &= \delta_{\{ij\}\{22\}}\delta_{\{kl\}\{11\}}, & T_{ijkl}^5 &= \delta_{\{ij\}\{33\}}\delta_{\{kl\}\{11\}}, & T_{ijkl}^6 &= \delta_{\{ij\}\{33\}}\delta_{\{kl\}\{22\}}, \\
T_{ijkl}^7 &= \frac{1}{\sqrt{2}}(\delta_{\{ij\}\{11\}}\delta_{\{kl\}\{23\}}), & T_{ijkl}^8 &= \frac{1}{\sqrt{2}}(\delta_{\{ij\}\{12\}}\delta_{\{kl\}\{33\}}), \\
T_{ijkl}^9 &= \frac{1}{\sqrt{2}}(\delta_{\{ij\}\{13\}}\delta_{\{kl\}\{22\}}), & T_{ijkl}^{10} &= \frac{1}{\sqrt{2}}(\delta_{\{ij\}\{23\}}\delta_{\{kl\}\{11\}}), \\
T_{ijkl}^{11} &= \frac{1}{\sqrt{2}}(\delta_{\{ij\}\{33\}}\delta_{\{kl\}\{12\}}), & T_{ijkl}^{12} &= \frac{1}{\sqrt{2}}(\delta_{\{ij\}\{22\}}\delta_{\{kl\}\{13\}}), \\
T_{ijkl}^{13} &= \frac{1}{2}(\delta_{\{ij\}\{11\}}\delta_{\{kl\}\{12\}} - \delta_{\{ij\}\{12\}}\delta_{\{kl\}\{22\}}), \\
T_{ijkl}^{14} &= \frac{1}{\sqrt{20}}(\delta_{\{ij\}\{11\}}\delta_{\{kl\}\{12\}} + \delta_{\{ij\}\{12\}}\delta_{\{kl\}\{22\}} - 2\delta_{\{ij\}\{13\}}\delta_{\{kl\}\{23\}}), \\
T_{ijkl}^{15} &= \frac{1}{2}(\delta_{\{ij\}\{11\}}\delta_{\{kl\}\{13\}} - \delta_{\{ij\}\{13\}}\delta_{\{kl\}\{33\}}), \\
T_{ijkl}^{16} &= \frac{1}{\sqrt{20}}(\delta_{\{ij\}\{11\}}\delta_{\{kl\}\{13\}} + \delta_{\{ij\}\{13\}}\delta_{\{kl\}\{33\}} - 2\delta_{\{ij\}\{12\}}\delta_{\{kl\}\{23\}}), \\
T_{ijkl}^{17} &= \frac{1}{2}(\delta_{\{ij\}\{12\}}\delta_{\{kl\}\{11\}} - \delta_{\{ij\}\{22\}}\delta_{\{kl\}\{12\}}), \\
T_{ijkl}^{18} &= \frac{1}{\sqrt{20}}(\delta_{\{ij\}\{12\}}\delta_{\{kl\}\{11\}} + \delta_{\{ij\}\{22\}}\delta_{\{kl\}\{12\}} - 2\delta_{\{ij\}\{23\}}\delta_{\{kl\}\{13\}}),
\end{aligned}$$

$$\begin{aligned}
T_{ijkl}^{19} &= \frac{1}{2} (\delta_{\{ij\}\{22\}}\delta_{\{kl\}\{23\}} - \delta_{\{ij\}\{23\}}\delta_{\{kl\}\{33\}}) , \\
T_{ijkl}^{20} &= \frac{1}{\sqrt{20}} (\delta_{\{ij\}\{22\}}\delta_{\{kl\}\{23\}} + \delta_{\{ij\}\{23\}}\delta_{\{kl\}\{33\}} - 2\delta_{\{ij\}\{12\}}\delta_{\{kl\}\{13\}}) , \\
T_{ijkl}^{21} &= \frac{1}{2} (\delta_{\{ij\}\{13\}}\delta_{\{kl\}\{11\}} - \delta_{\{ij\}\{33\}}\delta_{\{kl\}\{13\}}) , \\
T_{ijkl}^{22} &= \frac{1}{\sqrt{20}} (\delta_{\{ij\}\{13\}}\delta_{\{kl\}\{11\}} + \delta_{\{ij\}\{33\}}\delta_{\{kl\}\{13\}} - 2\delta_{\{ij\}\{23\}}\delta_{\{kl\}\{12\}}) , \\
T_{ijkl}^{23} &= \frac{1}{2} (\delta_{\{ij\}\{23\}}\delta_{\{kl\}\{22\}} - \delta_{\{ij\}\{33\}}\delta_{\{kl\}\{23\}}) , \\
T_{ijkl}^{24} &= \frac{1}{\sqrt{20}} (\delta_{\{ij\}\{23\}}\delta_{\{kl\}\{22\}} + \delta_{\{ij\}\{33\}}\delta_{\{kl\}\{23\}} - 2\delta_{\{ij\}\{13\}}\delta_{\{kl\}\{12\}}) , \\
T_{ijkl}^{25} &= \frac{1}{\sqrt{10}} (\delta_{\{ij\}\{11\}}\delta_{\{kl\}\{11\}} - \delta_{\{ij\}\{22\}}\delta_{\{kl\}\{22\}} - \delta_{\{ij\}\{13\}}\delta_{\{kl\}\{13\}} + \delta_{\{ij\}\{23\}}\delta_{\{kl\}\{23\}}) , \\
T_{ijkl}^{26} &= \frac{1}{\sqrt{30}} (\delta_{\{ij\}\{11\}}\delta_{\{kl\}\{11\}} + \delta_{\{ij\}\{22\}}\delta_{\{kl\}\{22\}} - 2\delta_{\{ij\}\{33\}}\delta_{\{kl\}\{33\}} \\
&\quad - 2\delta_{\{ij\}\{12\}}\delta_{\{kl\}\{12\}} + \delta_{\{ij\}\{13\}}\delta_{\{kl\}\{13\}} + \delta_{\{ij\}\{23\}}\delta_{\{kl\}\{23\}}) , \\
T_{ijkl}^{27} &= \frac{1}{\sqrt{24}} (2\delta_{\{ij\}\{11\}}\delta_{\{kl\}\{11\}} + 2\delta_{\{ij\}\{22\}}\delta_{\{kl\}\{22\}} + 2\delta_{\{ij\}\{33\}}\delta_{\{kl\}\{33\}} \\
&\quad - \delta_{\{ij\}\{12\}}\delta_{\{kl\}\{12\}} - \delta_{\{ij\}\{13\}}\delta_{\{kl\}\{13\}} - \delta_{\{ij\}\{23\}}\delta_{\{kl\}\{23\}}) .
\end{aligned} \tag{A6}$$

The 27-plet tensors obey the relation

$$\begin{aligned}
\sum_{\mu=1}^{27} T_{ijkl}^{\mu} T_{mnop}^{\mu} &= \frac{1}{4} (\delta_{im}\delta_{jn}\delta_{ko}\delta_{lp} + \delta_{im}\delta_{jn}\delta_{kp}\delta_{lo} \\
&\quad + \delta_{in}\delta_{jm}\delta_{ko}\delta_{lp} + \delta_{in}\delta_{jm}\delta_{kp}\delta_{lo}) \\
&\quad - \frac{1}{20} (\delta_{im}\delta_{jl}\delta_{ko}\delta_{np} + \delta_{im}\delta_{jl}\delta_{kp}\delta_{no} \\
&\quad + \delta_{in}\delta_{jl}\delta_{ko}\delta_{mp} + \delta_{in}\delta_{jl}\delta_{kp}\delta_{mo} \\
&\quad + \delta_{im}\delta_{lo}\delta_{jk}\delta_{np} + \delta_{im}\delta_{lp}\delta_{jk}\delta_{no} \\
&\quad + \delta_{in}\delta_{lo}\delta_{jk}\delta_{mp} + \delta_{in}\delta_{lp}\delta_{jk}\delta_{mo} \\
&\quad + \delta_{il}\delta_{jm}\delta_{ko}\delta_{np} + \delta_{il}\delta_{jm}\delta_{kp}\delta_{no} \\
&\quad + \delta_{il}\delta_{jn}\delta_{ko}\delta_{mp} + \delta_{il}\delta_{jn}\delta_{kp}\delta_{mo} \\
&\quad + \delta_{ik}\delta_{jm}\delta_{lo}\delta_{np} + \delta_{ik}\delta_{jm}\delta_{lp}\delta_{no} \\
&\quad + \delta_{ik}\delta_{jn}\delta_{lo}\delta_{mp} + \delta_{ik}\delta_{jn}\delta_{lp}\delta_{mo}) \\
&\quad + \frac{1}{40} (\delta_{ik}\delta_{jl}\delta_{mo}\delta_{np} + \delta_{ik}\delta_{jl}\delta_{mp}\delta_{no} \\
&\quad + \delta_{il}\delta_{jk}\delta_{mo}\delta_{np} + \delta_{il}\delta_{jk}\delta_{mp}\delta_{no}) .
\end{aligned} \tag{A7}$$

The basis used for the 28-plet representation is

$$\begin{aligned}
T_{ijklmn}^1 &= \delta_{\{ijklmn\}\{111111\}} , & T_{ijklmn}^2 &= \delta_{\{ijklmn\}\{222222\}} , \\
T_{ijklmn}^3 &= \delta_{\{ijklmn\}\{333333\}} , & T_{ijklmn}^4 &= \frac{1}{\sqrt{6}}\delta_{\{ijklmn\}\{111112\}} ,
\end{aligned}$$

$$\begin{aligned}
T_{ijklmn}^5 &= \frac{1}{\sqrt{6}} \delta_{\{ijklmn\}\{111113\}}, & T_{ijklmn}^6 &= \frac{1}{\sqrt{6}} \delta_{\{ijklmn\}\{222221\}}, \\
T_{ijklmn}^7 &= \frac{1}{\sqrt{6}} \delta_{\{ijklmn\}\{222223\}}, & T_{ijklmn}^8 &= \frac{1}{\sqrt{6}} \delta_{\{ijklmn\}\{333331\}}, \\
T_{ijklmn}^9 &= \frac{1}{\sqrt{6}} \delta_{\{ijklmn\}\{333332\}}, & T_{ijklmn}^{10} &= \frac{1}{\sqrt{15}} \delta_{\{ijklmn\}\{111122\}}, \\
T_{ijklmn}^{11} &= \frac{1}{\sqrt{15}} \delta_{\{ijklmn\}\{111133\}}, & T_{ijklmn}^{12} &= \frac{1}{\sqrt{15}} \delta_{\{ijklmn\}\{222211\}}, \\
T_{ijklmn}^{13} &= \frac{1}{\sqrt{15}} \delta_{\{ijklmn\}\{222233\}}, & T_{ijklmn}^{14} &= \frac{1}{\sqrt{15}} \delta_{\{ijklmn\}\{333311\}}, \\
T_{ijklmn}^{15} &= \frac{1}{\sqrt{15}} \delta_{\{ijklmn\}\{333322\}}, & T_{ijklmn}^{16} &= \frac{1}{\sqrt{20}} \delta_{\{ijklmn\}\{111222\}}, \\
T_{ijklmn}^{17} &= \frac{1}{\sqrt{20}} \delta_{\{ijklmn\}\{111333\}}, & T_{ijklmn}^{18} &= \frac{1}{\sqrt{20}} \delta_{\{ijklmn\}\{222333\}}, \\
T_{ijklmn}^{19} &= \frac{1}{\sqrt{30}} \delta_{\{ijklmn\}\{111123\}}, & T_{ijklmn}^{20} &= \frac{1}{\sqrt{30}} \delta_{\{ijklmn\}\{222213\}}, \\
T_{ijklmn}^{21} &= \frac{1}{\sqrt{30}} \delta_{\{ijklmn\}\{333312\}}, & T_{ijklmn}^{22} &= \frac{1}{\sqrt{60}} \delta_{\{ijklmn\}\{111223\}}, \\
T_{ijklmn}^{23} &= \frac{1}{\sqrt{60}} \delta_{\{ijklmn\}\{111332\}}, & T_{ijklmn}^{24} &= \frac{1}{\sqrt{60}} \delta_{\{ijklmn\}\{222113\}}, \\
T_{ijklmn}^{25} &= \frac{1}{\sqrt{60}} \delta_{\{ijklmn\}\{222331\}}, & T_{ijklmn}^{26} &= \frac{1}{\sqrt{60}} \delta_{\{ijklmn\}\{333112\}}, \\
T_{ijklmn}^{27} &= \frac{1}{\sqrt{60}} \delta_{\{ijklmn\}\{333221\}}, & T_{ijklmn}^{28} &= \frac{1}{\sqrt{90}} \delta_{\{ijklmn\}\{112233\}}.
\end{aligned} \tag{A8}$$

The 28-plet tensors obey the relation

$$\sum_{\mu=1}^{28} T_{ijklmn}^{\mu} T_{opqrst}^{\mu} = \frac{1}{6!} \delta_{\{ijklmn\}} \delta_{\{opqrst\}}. \tag{A9}$$

The basis used for the 35-plet representation is

$$\begin{aligned}
T_{ijklm}^1 &= \delta_{\{ijkl\}\{1111\}} \delta_{m3}, & T_{ijklm}^2 &= \delta_{\{ijkl\}\{1111\}} \delta_{m2}, \\
T_{ijklm}^3 &= \delta_{\{ijkl\}\{2222\}} \delta_{m3}, & T_{ijklm}^4 &= \delta_{\{ijkl\}\{2222\}} \delta_{m1}, \\
T_{ijklm}^5 &= \delta_{\{ijkl\}\{3333\}} \delta_{m2}, & T_{ijklm}^6 &= \delta_{\{ijkl\}\{3333\}} \delta_{m1}, \\
T_{ijklm}^7 &= \frac{1}{2} \delta_{\{ijkl\}\{1112\}} \delta_{m3}, & T_{ijklm}^8 &= \frac{1}{2} \delta_{\{ijkl\}\{1113\}} \delta_{m2}, \\
T_{ijklm}^9 &= \frac{1}{2} \delta_{\{ijkl\}\{1222\}} \delta_{m3}, & T_{ijklm}^{10} &= \frac{1}{2} \delta_{\{ijkl\}\{2223\}} \delta_{m1}, \\
T_{ijklm}^{11} &= \frac{1}{2} \delta_{\{ijkl\}\{1333\}} \delta_{m2}, & T_{ijklm}^{12} &= \frac{1}{2} \delta_{\{ijkl\}\{2333\}} \delta_{m1}, \\
T_{ijklm}^{13} &= \frac{1}{\sqrt{6}} \delta_{\{ijkl\}\{1122\}} \delta_{m3}, & T_{ijklm}^{14} &= \frac{1}{\sqrt{6}} \delta_{\{ijkl\}\{1133\}} \delta_{m2}, \\
T_{ijklm}^{15} &= \frac{1}{\sqrt{6}} \delta_{\{ijkl\}\{2233\}} \delta_{m1}, & &
\end{aligned}$$

$$\begin{aligned}
T_{ijklm}^{16} &= \frac{1}{\sqrt{24}} (\delta_{\{ijkl\}\{1231\}}\delta_{m1} - \delta_{\{ijkl\}\{1232\}}\delta_{m2}) , \\
T_{ijklm}^{17} &= \frac{1}{\sqrt{72}} (\delta_{\{ijkl\}\{1231\}}\delta_{m1} + \delta_{\{ijkl\}\{1232\}}\delta_{m2} - 2\delta_{\{ijkl\}\{1233\}}\delta_{m3}) , \\
T_{ijklm}^{18} &= \frac{1}{\sqrt{8}} (\delta_{\{ijkl\}\{1112\}}\delta_{m2} - \delta_{\{ijkl\}\{1113\}}\delta_{m3}) , \\
T_{ijklm}^{19} &= \frac{1}{\sqrt{12}} (\delta_{\{ijkl\}\{1112\}}\delta_{m2} + \delta_{\{ijkl\}\{1113\}}\delta_{m3} - 2\delta_{\{ijkl\}\{1111\}}\delta_{m1}) , \\
T_{ijklm}^{20} &= \frac{1}{\sqrt{8}} (\delta_{\{ijkl\}\{2221\}}\delta_{m1} - \delta_{\{ijkl\}\{2223\}}\delta_{m3}) , \\
T_{ijklm}^{21} &= \frac{1}{\sqrt{12}} (\delta_{\{ijkl\}\{2221\}}\delta_{m1} + \delta_{\{ijkl\}\{2223\}}\delta_{m3} - 2\delta_{\{ijkl\}\{2222\}}\delta_{m2}) , \\
T_{ijklm}^{22} &= \frac{1}{\sqrt{8}} (\delta_{\{ijkl\}\{3331\}}\delta_{m1} - \delta_{\{ijkl\}\{3332\}}\delta_{m2}) , \\
T_{ijklm}^{23} &= \frac{1}{\sqrt{12}} (\delta_{\{ijkl\}\{3331\}}\delta_{m1} + \delta_{\{ijkl\}\{3332\}}\delta_{m2} - 2\delta_{\{ijkl\}\{3333\}}\delta_{m3}) , \\
T_{ijklm}^{24} &= \frac{1}{\sqrt{18}} (\delta_{\{ijkl\}\{1122\}}\delta_{m2} - \delta_{\{ijkl\}\{1123\}}\delta_{m3}) , \\
T_{ijklm}^{25} &= \frac{1}{\sqrt{72}} (3\delta_{\{ijkl\}\{1121\}}\delta_{m1} - 2\delta_{\{ijkl\}\{1122\}}\delta_{m2} - 1\delta_{\{ijkl\}\{1123\}}\delta_{m3}) , \\
T_{ijklm}^{26} &= \frac{1}{\sqrt{18}} (\delta_{\{ijkl\}\{1133\}}\delta_{m3} - \delta_{\{ijkl\}\{1132\}}\delta_{m2}) , \\
T_{ijklm}^{27} &= \frac{1}{\sqrt{72}} (3\delta_{\{ijkl\}\{1131\}}\delta_{m1} - 2\delta_{\{ijkl\}\{1133\}}\delta_{m3} - 1\delta_{\{ijkl\}\{1132\}}\delta_{m2}) , \\
T_{ijklm}^{28} &= \frac{1}{\sqrt{18}} (\delta_{\{ijkl\}\{2211\}}\delta_{m1} - \delta_{\{ijkl\}\{2213\}}\delta_{m3}) , \\
T_{ijklm}^{29} &= \frac{1}{\sqrt{72}} (3\delta_{\{ijkl\}\{2212\}}\delta_{m2} - 2\delta_{\{ijkl\}\{2211\}}\delta_{m1} - 1\delta_{\{ijkl\}\{2213\}}\delta_{m3}) , \\
T_{ijklm}^{30} &= \frac{1}{\sqrt{18}} (\delta_{\{ijkl\}\{2233\}}\delta_{m3} - \delta_{\{ijkl\}\{2231\}}\delta_{m1}) , \\
T_{ijklm}^{31} &= \frac{1}{\sqrt{72}} (3\delta_{\{ijkl\}\{2232\}}\delta_{m2} - 2\delta_{\{ijkl\}\{2233\}}\delta_{m3} - 1\delta_{\{ijkl\}\{2231\}}\delta_{m1}) , \\
T_{ijklm}^{32} &= \frac{1}{\sqrt{18}} (\delta_{\{ijkl\}\{3311\}}\delta_{m1} - \delta_{\{ijkl\}\{3312\}}\delta_{m2}) , \\
T_{ijklm}^{33} &= \frac{1}{\sqrt{72}} (3\delta_{\{ijkl\}\{3313\}}\delta_{m3} - 2\delta_{\{ijkl\}\{3311\}}\delta_{m1} - 1\delta_{\{ijkl\}\{3312\}}\delta_{m2}) , \\
T_{ijklm}^{34} &= \frac{1}{\sqrt{18}} (\delta_{\{ijkl\}\{3322\}}\delta_{m2} - \delta_{\{ijkl\}\{3321\}}\delta_{m1}) , \\
T_{ijklm}^{35} &= \frac{1}{\sqrt{72}} (3\delta_{\{ijkl\}\{3323\}}\delta_{m3} - 2\delta_{\{ijkl\}\{3322\}}\delta_{m2} - 1\delta_{\{ijkl\}\{3321\}}\delta_{m1}) . \tag{A10}
\end{aligned}$$

The 35-plet tensors obey the relation

$$\begin{aligned}
\sum_{\mu=1}^{35} T_{ijklm}^{\mu} T_{nopqr}^{\mu} &= \frac{1}{24} \delta_{\{ijkl\}} \delta_{\{nopq\}} \delta_{mr} \\
&- \frac{1}{144} \left(\delta_{\{jkl\}} \delta_{\{opq\}} \delta_{im} \delta_{nr} + \delta_{\{jkl\}} \delta_{\{npq\}} \delta_{im} \delta_{or} \right. \\
&\quad + \delta_{\{jkl\}} \delta_{\{noq\}} \delta_{im} \delta_{pr} + \delta_{\{jkl\}} \delta_{\{nop\}} \delta_{im} \delta_{qr} \\
&\quad + \delta_{\{ikl\}} \delta_{\{opq\}} \delta_{jm} \delta_{nr} + \delta_{\{ikl\}} \delta_{\{npq\}} \delta_{jm} \delta_{or} \\
&\quad + \delta_{\{ikl\}} \delta_{\{noq\}} \delta_{jm} \delta_{pr} + \delta_{\{ikl\}} \delta_{\{nop\}} \delta_{jm} \delta_{qr} \\
&\quad + \delta_{\{ijl\}} \delta_{\{opq\}} \delta_{km} \delta_{nr} + \delta_{\{ijl\}} \delta_{\{npq\}} \delta_{km} \delta_{or} \\
&\quad + \delta_{\{ijl\}} \delta_{\{noq\}} \delta_{km} \delta_{pr} + \delta_{\{ijl\}} \delta_{\{nop\}} \delta_{km} \delta_{qr} \\
&\quad + \delta_{\{ijk\}} \delta_{\{opq\}} \delta_{lm} \delta_{nr} + \delta_{\{ijk\}} \delta_{\{npq\}} \delta_{lm} \delta_{or} \\
&\quad \left. + \delta_{\{ijk\}} \delta_{\{noq\}} \delta_{lm} \delta_{pr} + \delta_{\{ijk\}} \delta_{\{nop\}} \delta_{lm} \delta_{qr} \right). \quad (A11)
\end{aligned}$$

Appendix B: BUILDING THE OCTET OPERATORS

The construction of operators relies on textbook group theory methods (see, for example, Ref. [74]). Table VII is a reminder of the connection between angular momentum in the continuum and on a lattice[75, 76]. To build an octet operator, begin with a single chair and list all possible rotations of it. There are 24 orientations in total, as shown in Fig. 1. The A_1 representation is built from a particular sum,

$$H^{(8)\alpha}(A_1) = \left(\sum_{a=1}^{24} L_a^{(8)} \right)_{ij} T_{ij}^{\alpha}. \quad (B1)$$

Any octahedral rotation of this sum leaves it invariant, as expected for a $J = 0$ operator. The A_2 representation is built from a different sum,

$$H^{(8)\alpha}(A_2) = \left(\sum_{a=1}^{12} (-1)^a L_a^{(8)} - \sum_{a=13}^{24} (-1)^a L_a^{(8)} \right)_{ij} T_{ij}^{\alpha}. \quad (B2)$$

Some octahedral rotations of this sum leave it invariant; others return the negative of the sum. The T_1 representation is built from a set of three sums,

$$H^{(8)\alpha}(T_1^x) = \left(L_6^{(8)} + L_{20}^{(8)} + L_{21}^{(8)} + L_{11}^{(8)} - L_{18}^{(8)} - L_8^{(8)} - L_9^{(8)} - L_{23}^{(8)} \right)_{ij} T_{ij}^{\alpha}, \quad (B3)$$

$$H^{(8)\alpha}(T_1^y) = \left(L_5^{(8)} + L_{19}^{(8)} + L_{24}^{(8)} + L_{10}^{(8)} - L_{17}^{(8)} - L_7^{(8)} - L_{12}^{(8)} - L_{22}^{(8)} \right)_{ij} T_{ij}^{\alpha}, \quad (B4)$$

$$H^{(8)\alpha}(T_1^z) = \left(L_1^{(8)} + L_2^{(8)} + L_3^{(8)} + L_4^{(8)} - L_{13}^{(8)} - L_{14}^{(8)} - L_{15}^{(8)} - L_{16}^{(8)} \right)_{ij} T_{ij}^{\alpha}. \quad (B5)$$

Any octahedral rotation of one of these sums returns one of the three sums (itself or one of the other two) up to ± 1 , as expected for a vector with $J = 1$. The T_2 representation is built from a set of three sums,

$$H^{(8)\alpha}(T_2^x) = \left(L_6^{(8)} - L_{20}^{(8)} + L_{21}^{(8)} - L_{11}^{(8)} + L_{18}^{(8)} - L_8^{(8)} + L_9^{(8)} - L_{23}^{(8)} \right)_{ij} T_{ij}^{\alpha}, \quad (B6)$$

$$H^{(8)\alpha}(T_2^y) = \left(L_5^{(8)} - L_{19}^{(8)} + L_{24}^{(8)} - L_{10}^{(8)} + L_{17}^{(8)} - L_7^{(8)} + L_{12}^{(8)} - L_{22}^{(8)} \right)_{ij} T_{ij}^\alpha, \quad (\text{B7})$$

$$H^{(8)\alpha}(T_2^z) = \left(L_1^{(8)} - L_2^{(8)} + L_3^{(8)} - L_4^{(8)} + L_{13}^{(8)} - L_{14}^{(8)} + L_{15}^{(8)} - L_{16}^{(8)} \right)_{ij} T_{ij}^\alpha. \quad (\text{B8})$$

Any octahedral rotation of one of these sums returns one of the three sums (itself or one of the other two) up to ± 1 . The E representation is built from a set of three differences,

$$v_1 - v_2, \quad (\text{B9})$$

$$v_2 - v_3, \quad (\text{B10})$$

$$v_3 - v_1, \quad (\text{B11})$$

where

$$v_1 \equiv \left(L_6^{(8)} + L_{20}^{(8)} + L_{21}^{(8)} + L_{11}^{(8)} + L_{18}^{(8)} + L_8^{(8)} + L_9^{(8)} + L_{23}^{(8)} \right)_{ij} T_{ij}^\alpha, \quad (\text{B12})$$

$$v_2 \equiv \left(L_5^{(8)} + L_{19}^{(8)} + L_{24}^{(8)} + L_{10}^{(8)} + L_{17}^{(8)} + L_7^{(8)} + L_{12}^{(8)} + L_{22}^{(8)} \right)_{ij} T_{ij}^\alpha, \quad (\text{B13})$$

$$v_3 \equiv \left(L_1^{(8)} + L_2^{(8)} + L_3^{(8)} + L_4^{(8)} + L_{13}^{(8)} + L_{14}^{(8)} + L_{15}^{(8)} + L_{16}^{(8)} \right)_{ij} T_{ij}^\alpha. \quad (\text{B14})$$

Notice that only two of the three differences are linearly independent. Any octahedral rotation of one of these differences returns one of the three differences (itself or one of the other two) up to ± 1 .

The next task is to calculate the character χ of each representation, which is defined to be the set of traces of the explicit matrix representation. Since the octahedral group has five conjugacy classes, we need to evaluate five traces per representation. To be explicit, we can use

$$\left\{ \chi(e), \chi(c_2^{(xy)}), \chi(c_3^{(x \rightarrow y \rightarrow z \rightarrow x)}), \chi(c_4^{(z)}), \chi\left(\left(c_4^{(z)}\right)^2\right) \right\} \quad (\text{B15})$$

where $c_2^{(xy)}$ denotes a 180° rotation about the line $(x + y = 1, z = 0)$ and $c_3^{(x \rightarrow y \rightarrow z \rightarrow x)}$ denotes a 120° rotation about the line $(x = y = z)$.

For the A_1 , A_2 , T_1 , and T_2 representations, it is not necessary to build an explicit matrix representation; we can merely sum the ± 1 factors for those rotations that return an element to \pm (itself). For the E representation it is best to build the two-dimensional matrices

TABLE VII: The relationship between continuum angular momentum J and octahedral irreducible representation Λ .

Λ	J				
	0	1	2	3	...
A_1	1	0	0	0	...
A_2	0	0	0	1	...
E	0	0	1	0	...
T_1	0	1	0	1	...
T_2	0	0	1	1	...

explicitly. A convenient choice for the basis (as used, for example, in Ref. [77]) is

$$\begin{pmatrix} H^{(8)\alpha}(E^1) \\ H^{(8)\alpha}(E^2) \end{pmatrix} = \begin{pmatrix} \frac{1}{\sqrt{2}}(v_1 - v_2) \\ \frac{-1}{\sqrt{6}}(v_1 + v_2 - 2v_3) \end{pmatrix} \quad (\text{B16})$$

and it leads to

$$e = \begin{pmatrix} 1 & 0 \\ 0 & 1 \end{pmatrix}, \quad (\text{B17})$$

$$c_4^{(z)} = \begin{pmatrix} -1 & 0 \\ 0 & 1 \end{pmatrix}. \quad (\text{B18})$$

Under a $c_4^{(y)}$ rotation, we obtain

$$\frac{1}{\sqrt{2}}(v_1 - v_2) \rightarrow \frac{1}{\sqrt{2}}(v_3 - v_2) \quad (\text{B19})$$

$$= \frac{1}{2} \left(\frac{1}{\sqrt{2}}(v_1 - v_2) \right) + \frac{\sqrt{3}}{2} \left(\frac{-1}{\sqrt{6}}(v_1 + v_2 - 2v_3) \right) \quad (\text{B20})$$

$$\frac{-1}{\sqrt{6}}(v_1 + v_2 - 2v_3) \rightarrow \frac{-1}{\sqrt{6}}(v_3 + v_2 - 2v_1) \quad (\text{B21})$$

$$= \frac{\sqrt{3}}{2} \left(\frac{1}{\sqrt{2}}(v_1 - v_2) \right) - \frac{1}{2} \left(\frac{-1}{\sqrt{6}}(v_1 + v_2 - 2v_3) \right). \quad (\text{B22})$$

Therefore

$$c_4^{(y)} = \begin{pmatrix} \frac{1}{2} & \frac{\sqrt{3}}{2} \\ \frac{\sqrt{3}}{2} & -\frac{1}{2} \end{pmatrix}. \quad (\text{B23})$$

All other matrices can be obtained by multiplication of $c_4^{(y)}$ and $c_4^{(z)}$ in various orders finding, for example,

$$c_2^{(xy)} = \begin{pmatrix} -1 & 0 \\ 0 & 1 \end{pmatrix}, \quad (\text{B24})$$

$$c_3^{(x \rightarrow y \rightarrow z \rightarrow x)} = \begin{pmatrix} -\frac{1}{2} & -\frac{\sqrt{3}}{2} \\ \frac{\sqrt{3}}{2} & -\frac{1}{2} \end{pmatrix}, \quad (\text{B25})$$

$$\left(c_4^{(z)} \right)^2 = \begin{pmatrix} 1 & 0 \\ 0 & 1 \end{pmatrix}. \quad (\text{B26})$$

The characters of all representations are collected into Table VIII, and the multiplicities are obtained through standard group theory methods:

$$m(A_1) = \frac{1}{24} \left(\chi(e) + 6\chi(c_2^{(xy)}) + 8\chi(c_3^{(x \rightarrow y \rightarrow z \rightarrow x)}) + 6\chi(c_4^{(z)}) + 3\chi((c_4^{(z)})^2) \right) = 1, \quad (\text{B27})$$

$$m(A_2) = \frac{1}{24} \left(\chi(e) - 6\chi(c_2^{(xy)}) + 8\chi(c_3^{(x \rightarrow y \rightarrow z \rightarrow x)}) - 6\chi(c_4^{(z)}) + 3\chi((c_4^{(z)})^2) \right) = 1, \quad (\text{B28})$$

$$m(E) = \frac{1}{24} \left(2\chi(e) - 8\chi(c_3^{(x \rightarrow y \rightarrow z \rightarrow x)}) + 6\chi((c_4^{(z)})^2) \right) = 1, \quad (\text{B29})$$

TABLE VIII: Characters χ of all irreducible representations Λ for the octet operator.

Λ	$\chi(e)$	$\chi(c_2^{(xy)})$	$\chi(c_3^{(x \rightarrow y \rightarrow z \rightarrow x)})$	$\chi(c_4^{(z)})$	$\chi((c_4^{(z)})^2)$
A_1	1	1	1	1	1
A_2	1	-1	1	-1	1
E	2	0	-1	0	2
T_1	3	-1	0	1	-1
T_2	3	1	0	-1	-1

$$m(T_1) = \frac{1}{24} \left(3\chi(e) - 6\chi(c_2^{(xy)}) + 6\chi(c_4^{(z)}) - 3\chi((c_4^{(z)})^2) \right) = 1, \quad (\text{B30})$$

$$m(T_2) = \frac{1}{24} \left(3\chi(e) + 6\chi(c_2^{(xy)}) - 6\chi(c_4^{(z)}) - 3\chi((c_4^{(z)})^2) \right) = 1. \quad (\text{B31})$$

To summarize, the operators that will be typed into the computer code are those shown in Eq. (13). Operators beyond the octet are built from this octet starting point, as described in Sec. II B.

-
- [1] E. Del Nobile, R. Franceschini, D. Pappadopulo, and A. Strumia, Nucl. Phys. **B826**, 217 (2010) [arXiv:0908.1567 [hep-ph]].
 - [2] F. del Aguila, J. de Blas, and M. Perez-Victoria, J. High Energy Phys. 09 (2010) 033 [arXiv:1005.3998 [hep-ph]].
 - [3] T. Han, I. Lewis, and Z. Liu, J. High Energy Phys. 12 **2010** 085 [arXiv:1010.4309 [hep-ph]].
 - [4] J. Kumar, A. Rajaraman, and B. Thomas, Phys. Rev. D **84**, 115005 (2011) [arXiv:1108.3333 [hep-ph]].
 - [5] V. Ilisie and A. Pich, Phys. Rev. D **86**, 033001 (2012) [arXiv:1202.3420 [hep-ph]].
 - [6] Y. Kats and M. J. Strassler, J. High Energy Phys. 11 **2012** 097 [arXiv:1204.1119 [hep-ph]].
 - [7] E. Bertuzzo, P. A. N. Machado, and R. Zukanovich Funchal, J. High Energy Phys. 02 **2013** 086 [arXiv:1209.6359 [hep-ph]].
 - [8] E. Ma, Phys. Lett. **58B**, 442 (1975).
 - [9] G. Karl, Phys. Rev. D **14**, 2374 (1976).
 - [10] F. Wilczek and A. Zee, Phys. Rev. D **16**, 860 (1977).
 - [11] Y. J. Ng and S. H. H. Tye, Phys. Rev. Lett. **41**, 6 (1978).
 - [12] H. Georgi and S. L. Glashow, Nucl. Phys. **B159**, 29 (1979).
 - [13] C. B. Dover, T. K. Gaissner, and G. Steigman, Phys. Rev. Lett. **42**, 1117 (1979).
 - [14] W. J. Marciano, Phys. Rev. D **21**, 2425 (1980).
 - [15] B. Holdom and M. E. Peskin, Nucl. Phys. **B208**, 397 (1982).
 - [16] K. Konishi and R. Tripiccionne, Phys. Lett. **121B**, 403 (1983).
 - [17] D. Lust, E. Papantonopoulos, K. H. Streng, and G. Zoupanos, Nucl. Phys. **B268**, 49 (1986).
 - [18] E. Braaten, A. R. White, and C. R. Willcox, Int. J. Mod. Phys. A **01**, 693 (1986).
 - [19] T. E. Clark, C. N. Leung, S. T. Love, and J. L. Rosner, Phys. Lett. B **177**, 413 (1986).
 - [20] G. V. Borisov, Y. F. Pirogov, and K. R. Rudakov, Z. Phys. C **36**, 217 (1987).
 - [21] A. R. White, Mod. Phys. Lett. A **02**, 945 (1987).

- [22] K. Fukazawa, T. Muta, J. Saito, I. Watanabe, M. Yonezawa, and M. Inoue, *Prog. Theor. Phys.* **85**, 111 (1991).
- [23] R. S. Chivukula, M. Golden, and E. H. Simmons, *Phys. Lett. B* **257**, 403 (1991).
- [24] R. S. Chivukula, M. Golden, and E. H. Simmons, *Nucl. Phys.* **B363**, 83 (1991).
- [25] T. Kahara, M. Ruggieri, and K. Tuominen, *Phys. Rev. D* **85**, 094020 (2012) [arXiv:1202.1769 [hep-ph]].
- [26] J. B. Kogut, J. Shigemitsu, and D. K. Sinclair, *Phys. Lett.* **145B**, 239 (1984).
- [27] E. Gerstenmayer, M. Faber, W. Feilmair, H. Markum, and M. Muller, *Phys. Lett. B* **231**, 453 (1989).
- [28] F. Karsch and M. Lutgemeier, *Nucl. Phys.* **B550**, 449 (1999) [hep-lat/9812023].
- [29] F. Basile, A. Pelissetto, and E. Vicari, *J. High Energy Phys.* 02 **2005** 044 [hep-th/0412026].
- [30] J. Engels, S. Holtmann, and T. Schulze, *Nucl. Phys.* **B724**, 357 (2005) [hep-lat/0505008].
- [31] G. Cossu, M. D'Elia, A. Di Giacomo, G. Lacagnina, and C. Pica, *Phys. Rev. D* **77**, 074506 (2008) [arXiv:0802.1795 [hep-lat]].
- [32] G. Cossu and M. D'Elia, *J. High Energy Phys.* 07 **2009** 048 [arXiv:0904.1353 [hep-lat]].
- [33] Y. Shamir, B. Svetitsky, and T. DeGrand, *Phys. Rev. D* **78**, 031502 (2008) [arXiv:0803.1707 [hep-lat]].
- [34] J. B. Kogut and D. K. Sinclair, *Phys. Rev. D* **81**, 114507 (2010) [arXiv:1002.2988 [hep-lat]].
- [35] J. B. Kogut and D. K. Sinclair, *Phys. Rev. D* **84**, 074504 (2011) [arXiv:1105.3749 [hep-lat]].
- [36] J. B. Kogut and D. K. Sinclair, *Phys. Rev. D* **85**, 054505 (2012) [arXiv:1111.3353 [hep-lat]].
- [37] T. DeGrand, Y. Shamir, and B. Svetitsky, *Phys. Rev. D* **87**, 074507 (2013) arXiv:1201.0935 [hep-lat].
- [38] Z. Fodor, K. Holland, J. Kuti, D. Negradi, C. Schroeder, and C. H. Wong, *Phys. Lett. B* **718**, 657 (2012) [arXiv:1209.0391 [hep-lat]].
- [39] D. K. Sinclair and J. B. Kogut, *Proc. Sci. LATTICE2012* (**2012**) 026 [arXiv:1211.0712 [hep-lat]].
- [40] T. DeGrand, Y. Shamir, and B. Svetitsky, *Phys. Rev. D* **88**, 054505 (2013) [arXiv:1307.2425 [hep-lat]].
- [41] T. DeGrand, Y. Shamir, and B. Svetitsky, *Phys. Rev. D* **79**, 034501 (2009) [arXiv:0812.1427 [hep-lat]].
- [42] T. DeGrand, Y. Shamir, and B. Svetitsky, *Phys. Rev. D* **82**, 054503 (2010) [arXiv:1006.0707 [hep-lat]].
- [43] N. A. Campbell, I. H. Jorjys, and C. Michael, *Phys. Lett.* **167B**, 91 (1986).
- [44] I. H. Jorjys and C. Michael, *Nucl. Phys.* **B302**, 448 (1988).
- [45] C. Michael, *Nucl. Phys. Proc. Suppl.* **26**, 417 (1992).
- [46] M. Foster and C. Michael (UKQCD Collaboration), *Phys. Rev. D* **59**, 094509 (1999) [hep-lat/9811010].
- [47] G. Karl and J. E. Paton, *Phys. Rev. D* **60**, 034015 (1999) [hep-ph/9904407].
- [48] Y. A. Simonov, *Nucl. Phys.* **B592**, 350 (2000) [hep-ph/0003114].
- [49] P. Guo, A. P. Szczepaniak, G. Galata, A. Vassallo, and E. Santopinto, *Phys. Rev. D* **77**, 056005 (2008) [arXiv:0707.3156 [hep-ph]].
- [50] F. Buisseret, *Eur. Phys. J. A* **38**, 233 (2008) [arXiv:0808.2399 [hep-ph]].
- [51] G. S. Bali and A. Pineda, *Phys. Rev. D* **69**, 094001 (2004) [hep-ph/0310130].
- [52] N. Brambilla, A. Pineda, J. Soto, and A. Vairo, *Nucl. Phys.* **B566**, 275 (2000) [hep-ph/9907240].
- [53] C. Michael, *Nucl. Phys.* **B259**, 58 (1985).

- [54] J. Ambjorn, P. Olesen, and C. Peterson, Nucl. Phys. **B240**, 189 (1984).
- [55] L. Del Debbio, M. Faber, J. Greensite, and S. Olejnik, Phys. Rev. D **53**, 5891 (1996) [hep-lat/9510028].
- [56] G. S. Bali, Phys. Rep. **343**, 1 (2001) [hep-ph/0001312].
- [57] D. B. Lichtenberg, *The Standard Model of Elementary Particles* (Bibliopolis, Napoli, Italy, 1991).
- [58] H. Georgi, Front. Phys. **54**, 1 (1982).
- [59] A. Mykkanen, M. Panero, and K. Rummukainen, J. High Energy Phys. 05 **2012** 069 [arXiv:1202.2762 [hep-lat]].
- [60] S. Deldar, Phys. Rev. D **62**, 034509 (2000) [hep-lat/9911008].
- [61] G. S. Bali, Phys. Rev. D **62**, 114503 (2000) [hep-lat/0006022].
- [62] B. Lucini and M. Teper, J. High Energy Phys. 06 **2010** 050 [hep-lat/0103027].
- [63] L. Del Debbio and D. Diakonov, Phys. Lett. B **544**, 202 (2002) [hep-lat/0205015].
- [64] L. Del Debbio, H. Panagopoulos, and E. Vicari, J. High Energy Phys. 09 **2003** 034 [hep-lat/0308012].
- [65] A. Dumitru, Y. Hatta, J. Lenaghan, K. Orginos, and R. D. Pisarski, Phys. Rev. D **70**, 034511 (2004) [hep-th/0311223].
- [66] S. Gupta, K. Huebner, and O. Kaczmarek, Phys. Rev. D **77**, 034503 (2008) [arXiv:0711.2251 [hep-lat]].
- [67] C. Anzai, Y. Kiyo, and Y. Sumino, Nucl. Phys. **B838**, 28 (2010) [arXiv:1004.1562 [hep-ph]].
- [68] J. Greensite, B. Lucini, and A. Patella, Phys. Rev. D **83**, 125019 (2011) [arXiv:1101.5344 [hep-th]].
- [69] B. Lucini and M. Panero, Phys. Rep. **526**, 93 (2013) [arXiv:1210.4997 [hep-th]].
- [70] L. Del Debbio, A. Patella, and C. Pica, Phys. Rev. D **81**, 094503 (2010) [arXiv:0805.2058 [hep-lat]].
- [71] T. Ishikawa *et al.* (JLQCD Collaboration), Phys. Rev. D **78**, 011502 (2008) [arXiv:0704.1937 [hep-lat]].
- [72] C. Morningstar and M. J. Peardon, Phys. Rev. D **69**, 054501 (2004) [hep-lat/0311018].
- [73] B. Efron and R. J. Tibshirani, *An Introduction to the Bootstrap* (Chapman and Hall, CRC Press, London, 1993).
- [74] J. F. Cornwell, *Group Theory in Physics: An Introduction* (Academic Press, San Diego, 1997).
- [75] R. C. Johnson, Phys. Lett. **114B**, 147 (1982).
- [76] B. Berg and A. Billoire, Nucl. Phys. **B221**, 109 (1983).
- [77] R. G. Petry, D. Harnett, R. Lewis, and R. M. Woloshyn, Phys. Rev. D **78**, 074502 (2008) [arXiv:0803.4141 [hep-lat]].